

NON-DESTRUCTIVE EVALUATION OF DEFORMATION AND FRACTURE PROPERTIES OF MATERIALS USING STRESS-STRAIN MICROPROBE

K.L.MURTY¹, M.D.MATHEW¹, P.Q.MIRAGLIA¹, V.N.SHAH² AND F.M.HAGGAG³

¹North Carolina State University, Raleigh, NC 27695-7909

²Idaho National Engineering and Environmental Laboratory, Idaho Falls, ID 83415-3870

³Advanced Technology Corporation, 661 Emory Valley Road, Suite A, Oak Ridge, TN 37830

ABSTRACT

Tensile deformation and fracture properties of several metallic materials, welds, and their heat-affected-zones were determined non-destructively using the Stress-Strain Microprobe (SSM) system. The system is based on automated ball indentation (ABI) technique and involves strain-controlled multiple indentations at the same location on the material surface by a small spherical indenter. The technique permits evaluation of tensile deformation parameters such as yield strength, ultimate tensile strength, strength coefficient, and strain-hardening exponent, and a fracture energy parameter called indentation energy to fracture. ABI tests were conducted on carbon steels, stainless steels, nickel alloys, aluminum alloys, Zircalloys, electronic soldering materials and several nuclear pressure vessel steels (in the unirradiated, neutron irradiated, and irradiated and thermally annealed conditions). For all these test materials and conditions, the ABI-derived results were found to agree with the data from conventional standard test methods. In addition to the laboratory applications of SSM, it can be used as an in-situ testing instrument for non-destructive assessment of deformation and fracture properties of operating structural components.

INTRODUCTION

Techniques to characterize deformation and fracture behavior of components are needed to assess the degradation in properties and estimate remaining life of structures in various applications. While destructive tests using material removed from components do provide relevant data, in-situ measurements using non-destructive techniques on real structures are desirable. Another important criterion is that the technique should be capable of yielding these data using minimal amount of material so that gradient properties in welds and their heat-affected-zones (HAZ) can be evaluated. One such technique is the Automated Ball Indentation (ABI). While the idea of ball indentation is not new [1], ABI technique is unique because it incorporates fully automated measurement of impression parameters. It does not require measurement of diameter of the indentation using elaborate profilometry, optical interferometry, etc., which renders the traditional methodology unsuitable for on-line monitoring of the mechanical properties of components. Based on this principle, a portable/in-situ stress-strain microprobe system was developed recently by Advanced Technology Corporation [2] to test minimal material, and determine tensile properties (e.g. yield strength, tensile strength, strain-hardening exponent, strength coefficient) and fracture property (in terms of a fracture energy parameter called indentation energy to fracture, (IEF)). SSM system and the test methods incorporate known and accepted theoretical and empirical relationships governing material response to multiaxial indentation loading [3]. ABI is a relatively simple, rapid (~ few minutes)

and non-destructive technique, requires small amount of material with very little specimen preparation, and can be adopted for in-situ testing on real structures. Extension of this methodology can be made for high temperature studies, indentation fatigue, fracture and creep.

One of the advantages of ABI technique is that it is non-destructive since no material is removed from the specimen. A smooth shallow spherical indentation, less than 0.3 mm deep is left at the end of the test. This spherical impression is harmless to the tested structure because it has no sharp edges, and so it does not introduce any stress concentration sites. Figure 1 shows ABI indentations made with a 1.575 mm diameter ball indenter. Because of the small area over which the test is carried out, it is possible to determine point to point variations in mechanical properties, for example, between base metal, HAZ and weld nugget in a weldment. ABI technique is a state-of-the-art mechanical test that measures directly the local deformation (stress-strain) behavior of the material. Hence, in addition to the laboratory applications of SSM, it can be used as an in-situ testing instrument for non-destructive assessment of deformation and fracture properties of operating structural components (e.g. nuclear, chemical, aerospace, and defense) without adversely affecting their structural integrity.

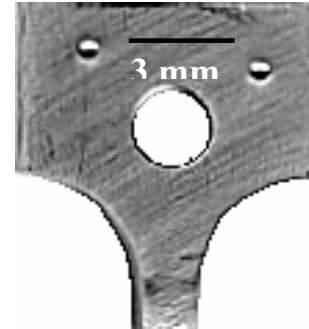


Fig.1.
ABI indentations on the shoulder of a broken tensile specimen.

We employed ABI technique to characterize tensile and fracture behavior of various materials such as carbon steels, nuclear pressure vessel steels, stainless steels, aluminum alloys, zircalloys, electronic solders, etc. Results obtained from ABI tests have been compared with data from tensile and Charpy impact tests. In this paper, we describe the ABI experimental and analytical procedures along with sample results on laboratory specimens using commercially available SSM system. Results from a new single-cycle ABI test procedure developed for high strain-rate testing and continuous stress-strain measurement in electronic solder materials (Sn5%Sb) are also presented. A brief description about the SSM system and its principles is included in the paper. Further details may be found elsewhere [4 - 6].

STRESS-STRAIN MICROPROBE

The SSM system uses an electro-mechanically driven indenter, high resolution penetration transducer and load cell, a personal computer (PC), a 16-bit data acquisition/control unit, and a copyrighted ABI software. The test is fully automated with a PC and test controller used in innovative ways to control the test and analyze data including real-time graphics, digital display of load-depth test data, etc. Figure 2 shows an overall view of a laboratory model (a) and a portable model for testing on components (b). Spherical indenters made of tungsten carbide are used with diameters varying from 0.254 mm to 1.575 mm, depending on the specimen thickness and width of the microstructural region to be tested. The indenter is driven at a constant speed into the test material, and progressive multiple loadings/partial unloadings are performed at the same test location. Indentation load, and depth of penetration are monitored using on-line load cell and linear variable differential transducer, respectively. Low and high temperature testing capability has been added recently with a furnace and temperature controller for testing in the range of $-200\text{ }^{\circ}\text{C}$ to $+200\text{ }^{\circ}\text{C}$. Figure 3 shows a typical indentation load versus depth of penetration curve.

ABI ANALYSIS

Yield Strength

In a standard tensile test, the uniaxial deformation is confined to the constant volume of the specimen's gauge section. Initially, the material is deformed elastically, following which plastic yielding and work-hardening commence and continue uniformly till the onset of necking. In contrast, in an ABI test, the loading is compressive; the elastic and plastic deformations are not distinctly separated. With increasing indentation penetration depth, an increasing volume of test material is forced to flow under multiaxial compressive stresses generated by the advancing indenter. Hence, in an ABI test, both elastic and plastic deformation take place simultaneously during the whole test. An accurate determination of yield strength should hence be based on the entire load-displacement curve from the ABI test. It should be emphasized that in an ABI test consisting of seven loading and unloading cycles, there will be seven consecutive processes of work hardening of both old and new material. Hence, the yield strength analysis is carried out by taking into account simultaneous occurrence of yielding and strain hardening of the material under conditions of multiaxial compression.

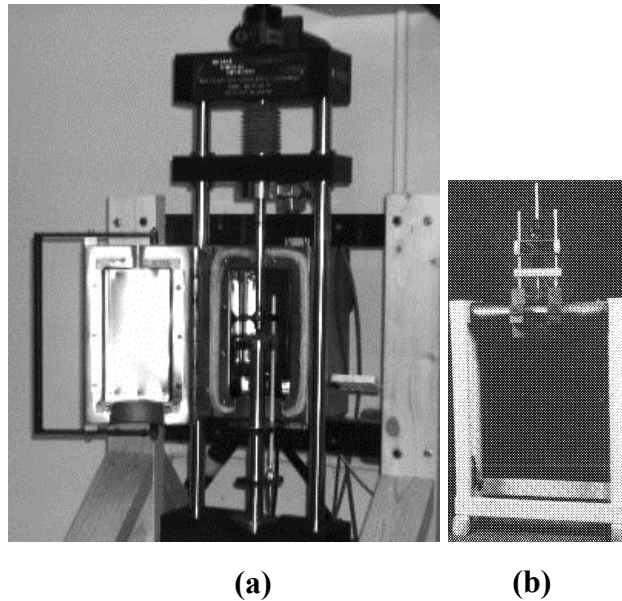


Figure 2
Overall view of ABI machine (a) laboratory model and (b) portable model for testing on components.

Figure 3 shows a schematic representation of the indentation profile in an ABI test. For each ABI loading cycle, the total penetration depth (h_t) is measured while the load is applied, and the depth is converted to a total indentation diameter (d_t) using the following equation:

$$d_t = 2\sqrt{Dh_t - h_t^2}, \quad (1)$$

In equation (1), D is the diameter of the indenter. Data points from all loading cycles (maximum value of $d_t/D = 1.0$) are fit by linear regression analysis to the following relationship:

$$P/d_t^2 = A(d_t/D)^{m-2}, \quad (2)$$

where P is the applied indentation load, m is the Meyer's coefficient and A is a material parameter obtained from the regression.

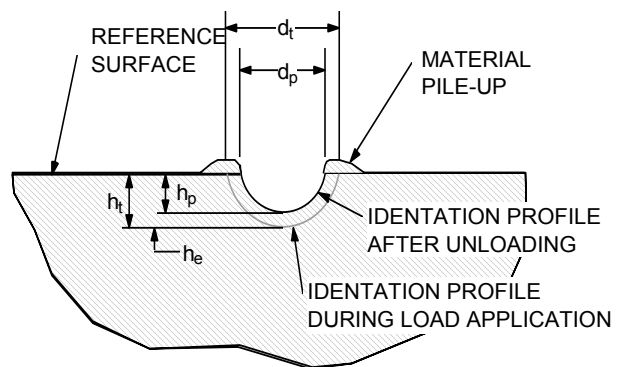


Figure 3
Schematic representation of the indentation profile in an ABI test.

Knowing the material parameter A, the yield strength (σ_y) is calculated from the expression:

$$\sigma_y = \beta_m A, \quad (3)$$

where β_m is a constant for a given class of materials. The value of β_m for each class of materials is determined independently using yield strength obtained from standard tensile tests, and value of A obtained from ABI tests. A single value of 0.2285 for β_m has been found to be applicable to all carbon steels whether cold rolled, hot rolled or irradiated [3,5].

ABI load increases approximately linearly with penetration depth as shown in Fig.4. The linear increase is the consequence of two non-linear processes occurring simultaneously, i.e. the non-linear increase in the applied load with penetration depth because of the spherical geometry of the indenter and increase in load required for further penetration because of work-hardening of the material. Hence, ABI tests do not exhibit the traditional segmented behavior, i.e., linear elastic followed by non-linear work-hardening of the material.

Stress-Strain Relation

A basic premise in the application of the ABI technique is that materials behave similarly under tensile and compressive loading. Plastic flow of materials is generally represented by the equation

$$\sigma_t = K \varepsilon_p^n, \quad (4)$$

where σ_t is the true stress, ε_p is the true plastic strain, n is the strain hardening exponent and K is the strength coefficient. This representation is not a necessary requirement for determining the indentation-derived σ_t - ε_p curve as

will be shown later (equations 6 and 7) but it can be used to determine n over the ε_p range of interest. Besides, a single power curve may not fit the entire flow curve as noted in ASTM Standard E646-78 (Standard Test Method for Tensile Strain Hardening Exponents of Metallic Sheet Materials).

A computer program is used to determine the true stress and true strain values. From the plastic depth h_p , the plastic diameter d_p is calculated by iterating the following equation,

$$d_p = \sqrt[3]{(2.735 P D) \frac{\left[\frac{1}{E_{spec}} + \frac{1}{E_{ind}} \right] \left[4h_p^2 + d_p^2 \right]}{4h_p^2 + d_p^2 - 4h_p D}}, \quad (5)$$

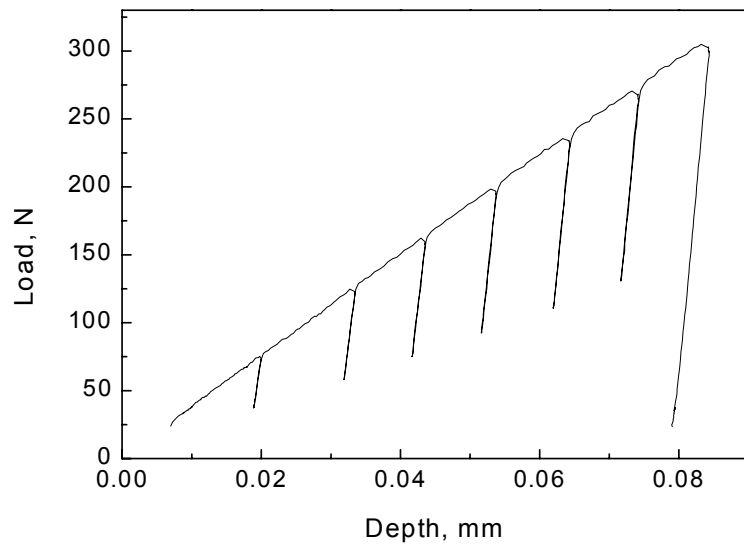


Figure 4
Typical indentation load versus depth of penetration curve

where P is the measured load, E_{spec} and E_{ind} are the elastic moduli of the specimen and indenter respectively. The true stress (σ_t) and plastic strain (ε_p) values are then calculated using the following equations,

$$\varepsilon_p = 0.2 \frac{d_p}{D}, \quad (6)$$

$$\sigma_t = \frac{4P}{\pi d_p^2 \delta}, \quad (7)$$

where δ is a parameter related to the constraint effect for plastic deformation. δ increases from a value of 1.12 at the initial yielding of the material up to a value near 3 at full plastic zone development. δ is calculated by the ABI software by iterating the following set of equations:

$$\delta = \begin{cases} (1) 1.12 & \phi \leq 1 \\ (2) 1.12 + \tau \cdot \ln \phi & 1 < \phi \leq 27, \text{ where } \tau = (2.87 \cdot \alpha_m - 1.12) / \ln(27), \text{ where } \phi = \varepsilon_p E_{spec} / 0.43 \sigma_t. \\ (3) 2.87 \cdot \alpha_m & \phi > 27 \end{cases} \quad (8)$$

There are three stages in the development of the plastic zone beneath the indentation and are expressed analytically in the δ parameter : (i) nucleation of a plastic zone during initial yielding, (ii) development of the zone with an increasing size as a function of ϕ , and (iii) full establishment of plasticity around the indentation as the zone is well developed and envelopes the indentation. The α_m parameter is material dependent and it varies between 0.90 and 1.25 for various structural steels, depending on the strain rate sensitivity and triaxial hardening.

Under compressive loading, the material does not undergo necking and so does not attain instability conditions. Hence the ultimate tensile stress is determined in an indirect way. Since n is equal to the true uniform strain at the ultimate tensile stress of the material under tensile loading, the true ultimate tensile stress can be obtained from Eq.(4) as

$$\sigma_{TS} = K(n)^n \quad (8a)$$

The ultimate tensile strength (nominal value), S_{UTS} , is then obtained from the equation

$$S_{UTS} = K \left(\frac{\varepsilon_u}{e} \right)^n = K \left(\frac{n}{e} \right)^n, e \approx 2.71 \quad (9)$$

Values of n and K are determined by regression analysis of the data fitted to Eq.(4).

Indentation Energy to Fracture

The stress-strain microprobe may also be used to estimate Charpy energy and fracture toughness of ductile materials. This particular use of the ABI technique is not apparent because indentation does not induce any cracking in the material. In addition, the stresses at the center of the contact surface of the test specimen under the indenter are compressive, whereas the stresses in front of a crack tip in a fracture specimen are tensile. It is assumed that although compressive loading does not promote fracture, it does introduce triaxiality in the material through the indentation process. Elasticity theory and preliminary computer analyses results show that the stress triaxilities present at a crack tip in a fracture toughness specimen and at the center of the contact surface under the indenter are similar [7,8]. Therefore, the material at the center of the

contact surface under the indenter experiences a degree of constraint similar to that experienced by the material at the crack tip. The deformation energy at the center of the impression is hence comparable to that at the front of a crack tip. Therefore, it has been postulated that the indentation energy per unit contact area upto a critical fracture stress is related to the fracture energy of a material in the transition region [9]. This parameter is referred to as Indentation Energy to Fracture (IEF), and it represents the fracture energy as determined from ABI-measured stress-strain curves upto either the critical fracture stress or strain, depending upon the controlling micromechanism causing fracture, which in turn depends on the test temperature. The concept of a critical fracture stress is applied to the transition region and the concept of a critical fracture strain is applied to the upper shelf region.

The IEF model assumes fracture conditions to occur if the stress produced by the ball indentation exceeds the material's critical cleavage fracture stress (σ_f). (In the case of HSLA steels, it has been established that the critical cleavage fracture stress is independent of temperature and heat-treatment [10]). Hence if the value of stress at the point of contact is known as a function of indentation depth, the depth at which the stress exceeded σ_f could be calculated. If the energy deposited in the material by the indenter could be determined as a function of the depth, then the energy deposited upto assumed fracture stress could be predicted. This energy to fracture is termed the Indentation Energy to Fracture [9].

Determination of IEF requires (i) relationship between ABI flow stress and indentation depth, (ii) relationship between ABI flow stress and normal pressure at the point of contact, (iii) value of the critical stress for cleavage fracture, and (iv) relationship between energy deposited into the material by the indenter and depth of penetration. The relationship between ABI flow stress and depth is easily obtained from ABI data since load versus depth data is converted into stress versus strain. This relationship is linear as shown in in Fig.3, thereby allowing easy extrapolation.

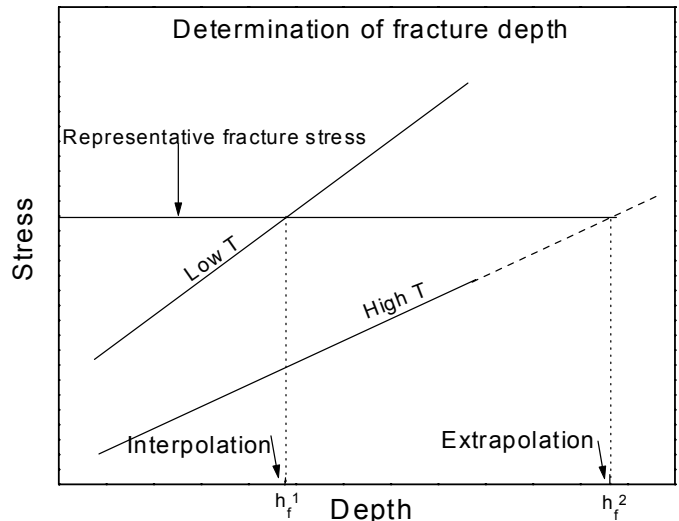


Figure 5
Schematic illustration of determination of fracture depth from indentation stress vs depth of penetration data at low and high temperatures.

Using elasticity theory, the ratio between ABI derived flow stress and the mean pressure at the point of contact was estimated to be approximately 2/3 [9]. This ratio was used to relate the critical fracture stress and a representative stress.

Instead of converting the flow stress into values of the mean pressure, σ_f was converted into an ABI flow stress called the *representative* fracture stress (σ_f^r) [9],

$$\sigma_f^r = \frac{2}{3} \sigma_f, \quad (10)$$

The representative stress, as defined in equation (10) is the critical stress to fracture normalized to ABI flow stress and intersects the flow curve regression line at a corresponding depth value as

shown in Fig.5. This depth delineates the point at which the stress state for fracture would exist ahead of the indenter and is termed “depth to fracture,” h_f . IEF, or the energy deposited into the material at the fracture depth is given as the integration of ABI flow stress up to the predicted depth to fracture. However, this energy is in the form of a surface energy, with units of energy per unit area (mJ/mm^2).

The derivation assumes that the flow stress is equal to the mean pressure, i.e., $\sigma_i = P/(\pi d^2/4)$. Load is equal to the slope of the load depth curve, m_{LD} , times the depth, i.e., $P = m_{LD} \cdot h$. Diameter of the impression is calculated from the depth of penetration using Pythagorean’s theorem, i.e., $d = 2\sqrt{Dh - h^2}$. The resultant expression for IEF is in terms of a natural logarithm of the depth to fracture as shown in Eq.(11),

$$IEF = \int_0^{h_f} \sigma_i(h) dh, \quad (11)$$

$$\text{Or, } IEF = \int_0^{h_f} \frac{m_{LD} \cdot h}{\pi \cdot (Dh - h^2)} dh = \frac{m_{LD}}{\pi} \cdot \ln \left[\frac{D}{(D - h_f)} \right] \quad (12)$$

RESULTS AND DISCUSSION

Steels, Welds and HAZs

ABI tests were performed on the shoulder portions of the tensile tested specimens of ASTM grade A533B steel which is commonly used in nuclear pressure vessels. Similar tests were also carried out on A212B steel that finds extensive application in reactor support structures. Figure 6 shows a comparison between ABI and tensile data for the two materials. Stress-strain curves determined by the two test methods showed a good correlation. Similar results have been obtained for other materials also such as a duplex austenitic stainless steel type CF8 (Fig.7). ABI tests were also conducted on laboratory specimens of spot welds from 1020 mild steel at three test locations, namely, base metal, HAZ, and weld metal. As seen from Fig. 8, the true-stress/true-plastic-strain curve of the HAZ is

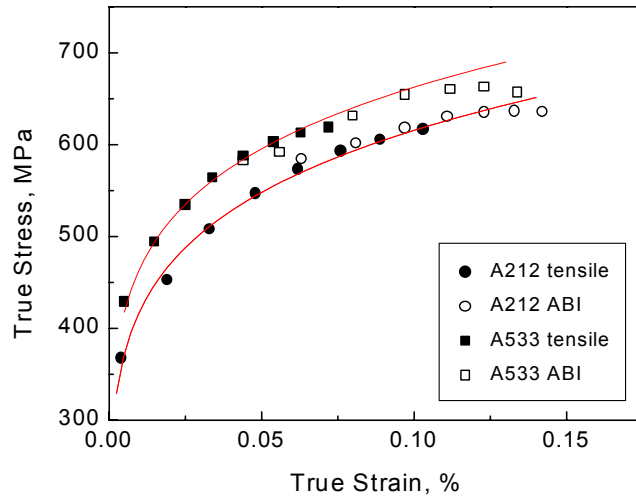


Figure 6
Correlation between ABI and tensile data for A212B and 533B steels.

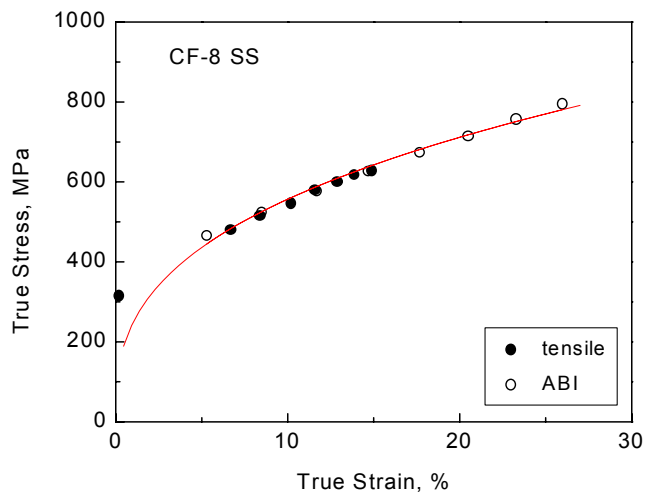


Figure 7
Correlation between ABI and tensile data for CF8 stainless steel.

bracketed by those from the base metal and weld metal. Similar studies on an A533B steel weld showed that HAZ has the highest strength whereas weld metal was similar to the base metal. These studies on welds have clearly demonstrated the ability of ABI technique to ascertain the relative strengths of different microstructural regions in a weld HAZ. The non-destructive aspect of the ABI technique allows testing welded joints with the presence of residual stress which is otherwise released in the process of making conventional tensile specimens. Furthermore, the localized ABI testing allows testing very narrow and/or irregular geometry HAZ areas. Hence, SSM system can be used for nondestructive, in-situ estimation of gradients in the stress-strain behavior of welded structural components. Figure 9 shows the variation of room temperature tensile strength across the base metal, weld metal and HAZ in an A533B weld. The microstructures of the three regions are also shown in the same Figure.

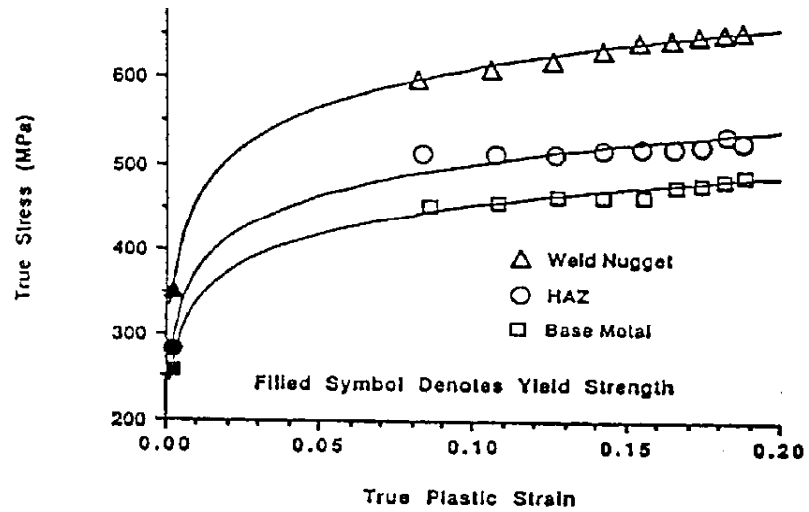


Figure 8
Comparison of stress-strain curves of base metal, weld nugget and HAZ of 1020 mild steel from ABI

Figure 9 shows the variation of room temperature tensile strength across the base metal, weld metal and HAZ in an A533B weld. The microstructures of the three regions are also shown in the same Figure.

Radiation Hardening and Post-Irradiation Annealing

The ABI technique was used to assess the degree of neutron-embrittlement damage and the percent recovery due to post-irradiation thermal annealing. Figure 10 depicts the true stress-strain curves for A533B pressure vessel steel in four conditions - unirradiated, neutron

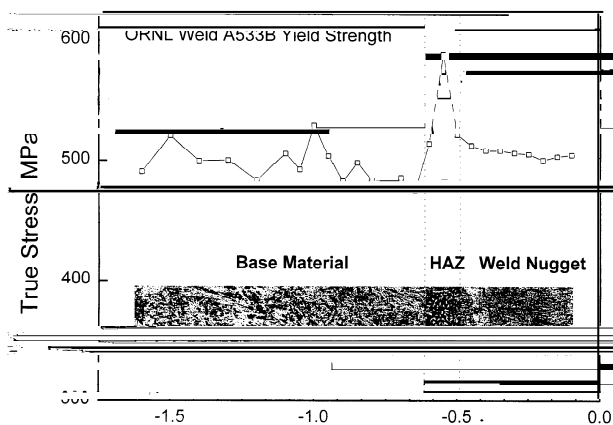


Figure 9
Gradient in room temperature tensile strength across base metal, weld metal and HAZ of A533B weld.

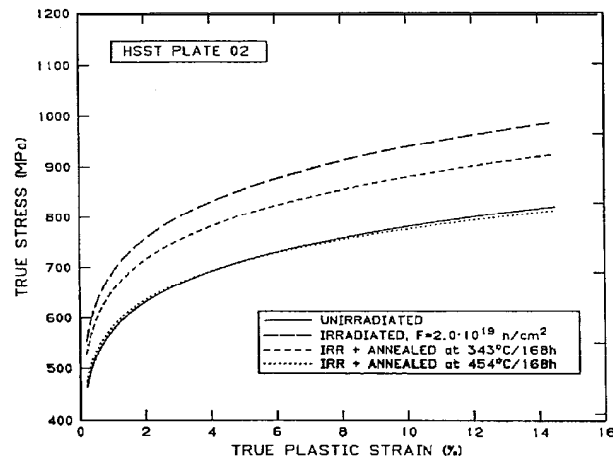


Figure 10
Comparison of ABI stress strain curves of A533B steel in unirradiated, irradiated, and irradiated plus annealed conditions.

irradiated to a fast fluence of 2×10^{18} n/cm², and two post-irradiated and thermally annealed conditions (for 168 h at 616 K and 726 K) and were in good agreement with the corresponding tensile results. These investigations demonstrate the capability of the SSM system to quantify the degree of embrittlement and recovery due to annealing of nuclear reactor pressure vessel steels. Furthermore, the SSM system can also monitor, non-destructively in-situ, the re-embrittlement rate of nuclear pressure vessels following thermal annealing during life-extension.

In-situ ABI Testing of Structural Components

As described earlier, Fig. 2(b) demonstrates the application of ABI for testing of actual components such as pipelines (100 mm outer diameter). The testing head of the portable/in-situ stress-strain microprobe system was clamped on the pipe using four 90 ° V-blocks. This

Table I. ABI results on Yield Strength (MPa) of 347 SS weld

Base Metal	Weld Metal	Heat Affected Zone
325	289	331

mounting method allowed the testing head to be rotated 360 ° and clamped rigidly for ABI testing at any location of the weld, HAZ, or the base metal. The ABI test results summarized in Table I show that the yield strength measured by the microprobe at the weld region is lower than those at the base metal and the HAZ. The above in-situ tests also successfully demonstrate the potential applicability of the microprobe system to non-destructively test full size welded pipes and pressure vessels.

Strain-rate-sensitivity (SRS) of Sn5%Sb solder

Sn5%Sb is one of the materials being considered for lead-free solder replacements in semiconductor electronic packaging applications. We used SSM to obtain load-depth curves in single cycle mode at varied indenter speeds. Figure 11 depicts the influence of strain-rate on the load-depth curves. Log-log plots of strain-rate versus stress are shown in Fig. 12 where the ABI

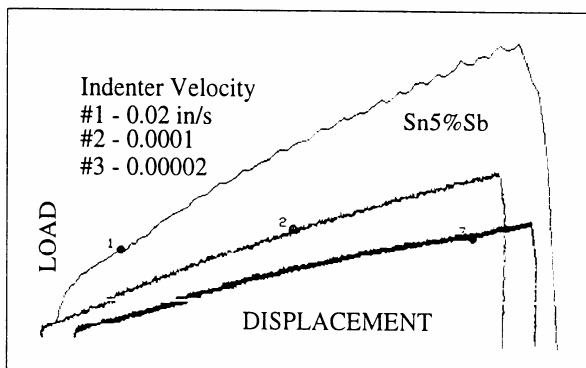


Figure 11
Influence of strain rate on the load-depth curves of Sn5%Sb.

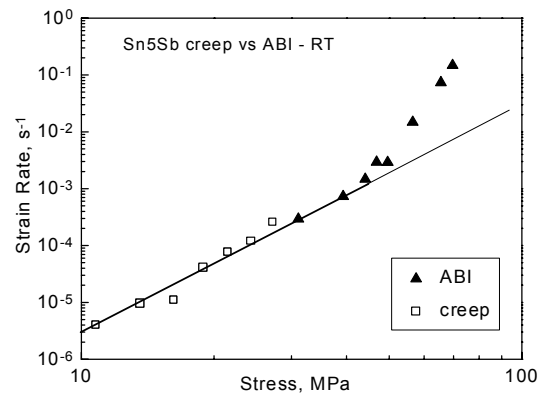


Figure 12
Variation of creep rate with stress; comparison of ABI and creep data.

results are plotted along with the creep data. In addition to the fact that the ABI test results are in reasonable agreement with creep data, these tests took about three hours time while they cover more than three orders of magnitude in strain rate whereas the creep tests were performed for a long period in excess of four months. Moreover, only one sample could be used to obtain this type of information using ABI/SSM.

Fracture Toughness

Figure 13 shows the variation of the ABI-specific toughness parameter, IEF, for an ASTM A533 grade weld metal as a function of temperature. The upper-shelf, lower-shelf and transition regions are clearly evident in this figure. These trends have been confirmed with Charpy data for this material, also plotted in the same figure [11]. It is suggested that IEF can be used as a parameter to determine shift in transition temperature and decrease in upper shelf energy due to embrittlement from aging, cold working and irradiation.

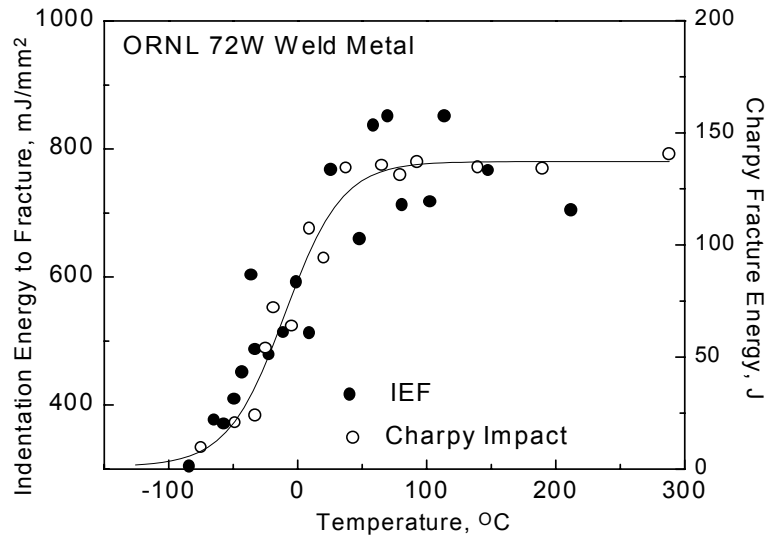


Figure 13
Variation of IEF and Charpy energy with temperature

SUMMARY

In summary, ABI is a relatively simple technique to characterize deformation and fracture properties of several materials (ferritic steels, stainless steels, electronic solders), welds and HAZs. The SSM system quantified the degree of neutron-embrittlement as well as the percentage recovery in mechanical properties resulting from post-irradiation thermal annealing of nuclear pressure vessel steels. Compared to conventional tests, ABI technique has many advantages with possible extensions to in-situ tests on real structures. Thus the method is useful in monitoring in-service mechanical property changes and the aging of bridges and other critical components and thus aid in verifying their structural integrity.

ACKNOWLEDGEMENT

This project has been funded by the INEEL University Research Consortium. The INEEL is managed by Lockheed Martin Idaho Technologies Company for the U.S. Department of Energy, Idaho Operations Office, under Contract No. DE-AC07-94ID13223.

REFERENCES

1. D. Tabor, *The Hardness of Metals*, Oxford University Press, New York (1951).
2. F. M. Haggag, *Field Indentation Microprobe for Structural Integrity Evaluation*, U.S. Patent No. 4,852,397, August 1, 1989.

3. F. M. Haggag, "In-Situ Measurements of Mechanical Properties Using Novel Automated Ball Indentation System," in *Small Specimen Test Techniques Applied to Nuclear Reactor Thermal Annealing and Plant Life Extension*, ASTM STP 1204, W. R. Corwin, F. M. Haggag, and W. L. Server, Eds., American Society for Testing and Materials, Philadelphia (1993) pp. 27-44.
4. F. M. Haggag, et al., "Use of Automated Ball Indentation Testing to Measure Flow Properties and Estimate Fracture Toughness in Metallic Materials," in *Applications of Automation Technology to Fatigue and Fracture Testing*, ASTM STP 1092, A. A. Braun, N. E. Ashbaugh, and F. M. Smith, Eds., American Society for Testing and Materials, Philadelphia (1990) pp. 188-208.
5. K.L. Murty and F.M. Haggag in *Proceedings of INTERPACK '97*, ASME, June 1997 (in print).
6. F.M. Haggag, "Application of Flow Properties Microprobe to Evaluate Gradients in Weldment Properties", in *Proceedings of the ASM 3rd International Conference on Trends in Welding Research*, ASM (1992) pp. 629 - 635.
7. S.P.Timoshenko and J.N.Goodier in *Theory of Plasticity*, 3rd edition, McGraw Hill, 1970, pp.409-414.
8. T.S.Byun, J.W.Kim and J.H.Hong, *Nuclear Technology*, (1998) (in print).
9. F.M. Haggag, Thak-Sang Byun, J.H. Hong, P.Q. Miraglia and K.L. Murty, *Scripta Met and Mater.*, **38** (1998) 645.
10. P. Bowen, S.G.Druce and J.F.Knott, *Acta Metallurgica*, **35** (1987) pp.1735-1746.
11. P. Q. Miraglia, The Automated Ball Indentation Technique and Its Application Towards Characterizing Mechanical and Fracture Properties of an RPV Weldment, M.S. Thesis, N. C. State University, 1997.

List of Figures

1. ABI indentations made with 1.575 mm diameter ball indenter on the shoulder region of a tensile specimen.
2. Overall view of ABI machine (a) laboratory model and (b) portable model for testing on components.
3. Schematic representation of the indentation profile in an ABI test.
4. Typical indentation load versus depth of penetration curve.
5. Determination of fracture depth from indentation stress versus depth of penetration data.
6. Correlation between ABI (symbols) and tensile (line) data for A533B and A212B steels.
7. Correlation between ABI (symbols) and tensile (line) data for CF8 stainless steel.
8. Comparison of stress-strain curves of base metal, weld nugget and HAZ of 1020 mild steel from ABI tests.
9. Gradient in room temperature tensile strength across base metal, weld nugget and HAZ of A533B weld.
10. Comparison of ABI-derived stress strain curves of A533B steel in unirradiated, irradiated, and irradiated plus annealed conditions.
11. Influence of strain rate on the load-depth curves of Sn5%Sb.
12. Variation of creep rate with stress -comparison between ABI and creep data.
13. Variation of IEF with temperature.